Surface Repair of Tool Made of 12 Ni Maraging Steel by Laser Cladding of NiCoMo Powder

Z. Bergant[1,a], J. Grum[1,b*], J.M.Slabe[2,c], J. L. Ocaña[3,d]
[1]University of Ljubljana, Faculty of Mechanical Engineering, Askerceva 6, Ljubljana, Slovenia
[2]Slovenian Technology Agency, Dunajska c. 22, Ljubljana, Slovenia
[3] Centro Láser U.P.M. Ctra deValencia, 28031 Madrid, Spain
[a]zoran.bergant@fs.uni-lj.si, [b]janez.grum@fs.uni-lj.si,
[c]janez.markoslabe@tia.si, [c]jlocana@etsii.upm.es
*corresponding author

Keywords: laser cladding, maraging steel, surface integrity, microhardness, residual stress

Abstract

Surface repair experiments with Nd:YAG coaxial laser cladding of NiCoMo maraging powder were made on specimens from maraging steel (EN 10027-2, mat. no. 1.2799). The influences of different modes of laser-beam guidance with various powder mass flows and with different degrees of overlapping of individual traces on the dilution and the repair area were determined. The micro and macroscopic analyses of microsections of fusion zone (FZ), heat affected zone (HAZ) and through-depth microhardness were analysed after cladding and after subsequent solution and precipitation annealing. The microchemical (EDS) analysis was performed at various depths. The residual stresses in the clad face and in the clad toe were determined and compared, using the hole-drilling method.

1. Introduction

Maraging steels are iron-nickel martensite steels with excellent mechanical properties, which can be attained by precipitation annealing, where molybdenum and titanium intermetallic compounds precipitate [1,2]. Laser cladding is subject of study by numerous authors [3-5]. Die casting tools are subjected to thermo-mechanical fatigue and erosion of melt which leads to local damages of the tool surface. The laser cladding is used to repair the damaged surface in order to extend the operating life of expensive dies. Grum and Slabe [6,7] studied the properties of maraging surfaced clads having different chemical compositions. The optimization of temperature-time condition of heat treatment was performed using response surface methodology (RSM). They reported that the microhardness values in clads with the same chemical composition are almost equal as in the forged material after solution and precipitation annealing. Shamantha et al [8] described characteristics of a microstructure of welded maraging steel, which can be characterised by three types of morphologies; from regular cellular, cellular-dendritic and at some sections, predominantly dendritic, especially at the vicinity of the fusion line. Vishwanathan et al [9] reported the detrimental influence of the retained austenite, generated through temperature fatigue, on mechanical properties of maraging steel.
The aim of the investigation was to analyze the properties of the laser clads on hot-working 12 Ni maraging tool steel. Influences of a changing of mode of laser-beam travel on the cross-sectional geometry of clads were analyzed with different percentages of laser-beam overlapping. In welding the tensile residual stresses in the weld face are obtained [10,11] due to temperature dilatation during solidification. Grum and Slabe [6] and Weiping [12] found that in multi-pass remelting and in multipass surfacing of martensite maraging steel the resulting residual stress is in compression due to the austenitic to martensitic phase transformation. Changes of microstructural and microchemical properties after laser cladding and after different time conditions of subsequent solution and precipitation annealing were studied.

2. Experimental procedure

2.1 Selection of the base and filler material

The experiments of laser cladding were carried out at specimens made of hot working maraging tool steel X 2 NiCoMoTi 12 8 8 (DIN), i.e. 1.2799 (Mat.No.), product of Edelstahl Witten-Krefeld GmbH (Germany). When delivered, the raw material was in a forged-solution annealed state. Maraging filler material NiCoMo shows a similar chemical composition in weight percentage. Iron was powder atomized in water, i.e. »Fersint«, product of Pometon, other alloying elements were agglomerated ground welding powders, Ni, Co, FeTi, NiMo, products of Elektrode Jesenice. Chemical compositions of the base material and filler materials are given in Table 1.

Table 1: Chemical composition (in wt.%) of maraging steel X 2 NiCoMoTi and NiCoMo powder

Material / Elements	Ni [%]	Co [%]	Mo [%]	Ti [%]	Al [%]	C [%]	Fe [%]
Maraging steel X2NiCoMoTi	12.0	8.0	8.0	0.5	0.05	0.02	71.73
NiCoMo powder	12.1	8.0	7.9	0.5	0.09	-	71.4

2.2 Laser cladding parameters

Laser cladding was carried out in Centro Laser of the Polytechnical University of Madrid, using 6-axis ABB robot. A laser cladding system with a 3.3 kW Nd:YAG laser and a robotic system for powder supply was used. Laser cladding parameters were: power P = 1150 W, travel speed v = 10 mm/s, laser spot diameter D_b = 3 mm, powder flow rate Q = 6 g/min, argon shielding gas Q = 20 l/min. The specimens were cladded using three different modes of laser-beam guidance (Mode I: continuous spiral, (b) Mode II: continuous zig-zag, (c) Mode III: intermittent line) with 20 % overlapping and two specimens with different degrees of overlapping, δ = 0 and 40 %. The cross section of single clad is elliptical; therefore, optimum overlapping of subsequent surfacing weld beads resulted in a relatively uniform surfacing-weld cross-sectional thickness.

2.3 Solution and precipitation annealing parameters

The specimens were cut into slices, which were then subsequently solution-annealed at 900 °C for 1 hour, precipitation-annealed at 525 °C for 1 hour, 2 hours, and 3 hours.

3. Analysis

3.1 Analysis of the geometry of the clad-beads macro sections.

Cross sections of cladded specimens were analysed. Figure 1 shows the plane of cutting. The specimens were cut in the middle in a direction perpendicular to the cladding direction. In order to evaluate the macro images at a magnification of 50 times, the images were put in a multiple image arrangement to capture a band zone of 20 mm x 1 mm.

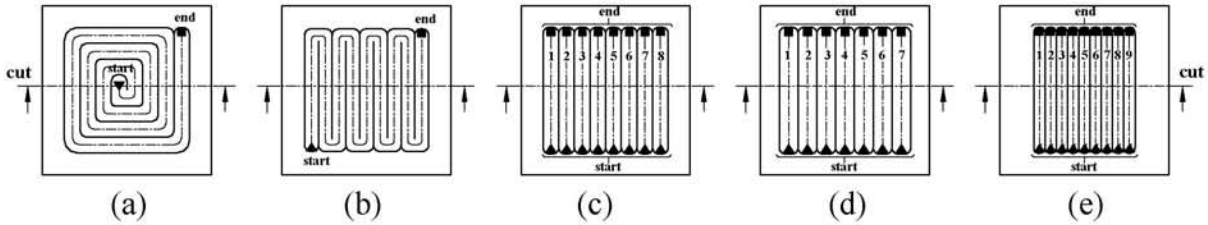

Fig 1: Selected scanning modes of laser-beam scanning across the specimen surface (a) Mode I: continuous spiral, (b) Mode II: zig-zag, (c) Mode III: intermittent line, *(d) Mode III: 0 % overlap, (e) Mode III: 40 % overlap*

The images were imported into AutoCad program, with which vector images of the cladded layer from the weld face to the fusion line with a known measure were produced.

Figure 2a shows cross-sectional dimensions of the single clad; width w, height h, depth penetration b, surface A , circumference P, penetration, and aspect ratio AR.
Figure 2b shows cross-sectional of several parallel clad-beads are surfaced. The first surfacing cladd-bead covers the next surfacing clad-bead; therefore, the width of filling surfacing clad-beads is smaller than the width of the initial surfacing clad-bead (w_1) and final surfacing clad-bead (w_n). Because of overlapping, the wetting angle between the first and final surfacing-clad beads is smaller. Parameter δ designates overlapping of clads.

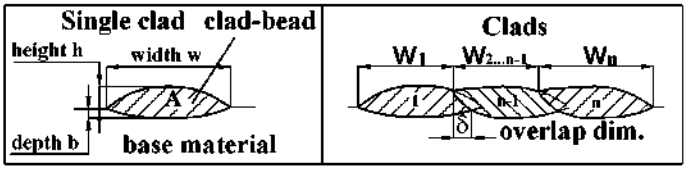

(a) (b)

Fig. 2. Geometrical dimensions of clad bead (a) single clad (b) overlapped clads

In Table 2 average values of the geometrical cross-sectional parameters of the clads at the specimens are given.

Table 2: Dimensions of clads – average values

Mode	Overlap [%]	Width w [μm]	Heigth h [μm]	Depth b [μm]	Dilution h/h+b	AR w/h	Area A [mm^2]	Perimeter P [mm]
I	20	2480	349,50	297,50	0,55	7,23	1,27	5,66
II	20	2500	348,67	331,89	0,51	7,24	1,39	6,24
III	20	2515	329,00	318,00	0,51	7,64	1,32	6,12
III	0	2978	330,43	299,57	0,52	9,04	1,33	6,23
III	40	1802	169,00	234,22	0,40	12,25	0,55	4,17

3.2 Hardness of the surfacing clads and base material

Figure 3a shows microhardness in a clad and the base material. Hardness in the clad cross-section ranges between 400 and 450 $HV_{0.3}$, a rapid decrease occurring close to the fusion line. In a depth ranging between 0.6 mm and 1 mm a softer HAZ with microhardness ranging between 300 and 350 $HV_{0.3}$ is located. In a depth ranging between 1.0 mm and 1.6 mm there is a harder HAZ with hardness values ranging by approximately 100 $HV_{0.3}$ higher, i.e. between 350 and 400 $HV_{0.3}$. In a depth of 1.6 mm there is a darker semicircular zone adjacent to the HAZ and the heat-unaffected zone. From a depth of 2 mm there is a heat-unaffected zone with uniform average hardness of 344 $HV_{0.3}$.
Figure 3b shows a microhardness variation in the clad and the base material after 1h solution annealing at 900 °C and after 3h precipitation annealing at 525 °C. Because of precipitation hardening the average hardness values in the clad and the base material increased.

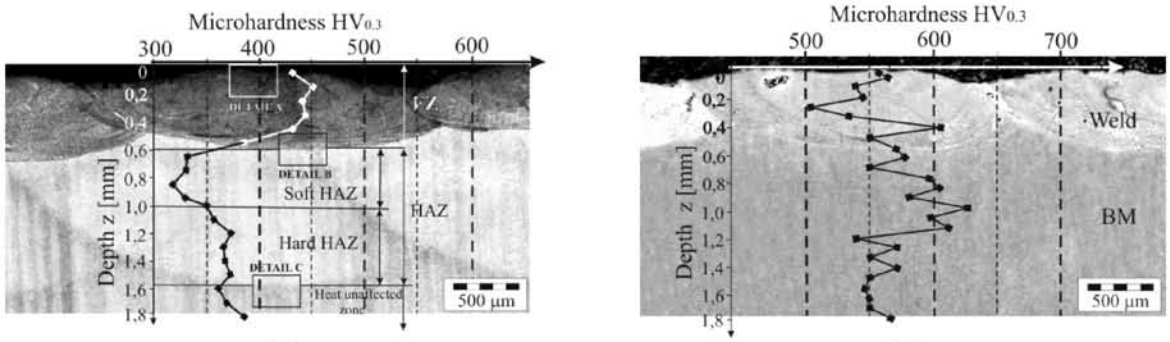

Fig. 3. Microhardness of specimen (a) after laser cladding etched for 20 sec. in 10 % nital, (b) after subsequent solution and precipitation annealing, etched for 3-5 sec. in 10 % nital

3.3 Microstructural and microchemical analyses

The metallographic specimens were inserted into graphite powder and prepared in accordance with a standard procedure. They were polished with polycrystalline diamond with grains of 3 µm, i.e. 1 µm in distilled water. Etching of the substrate was perfomed with 10 % nital. Figure 4a shows a surface of a NiCoMo weld after laser cladding. The cellular-dendritic microstructure is visible. Figure 4b shows a microstructure at a sharply defined fusion line, i.e. fusion zone/HAZ boundary. The orientation of dendrites is primarily perpendicular to the fusion line. Close to the fusion line dendrites are more frequent than the cellular microstructure. This can be attributed to rapid cooling rate due to the faster heat sink into the surrounding base material.

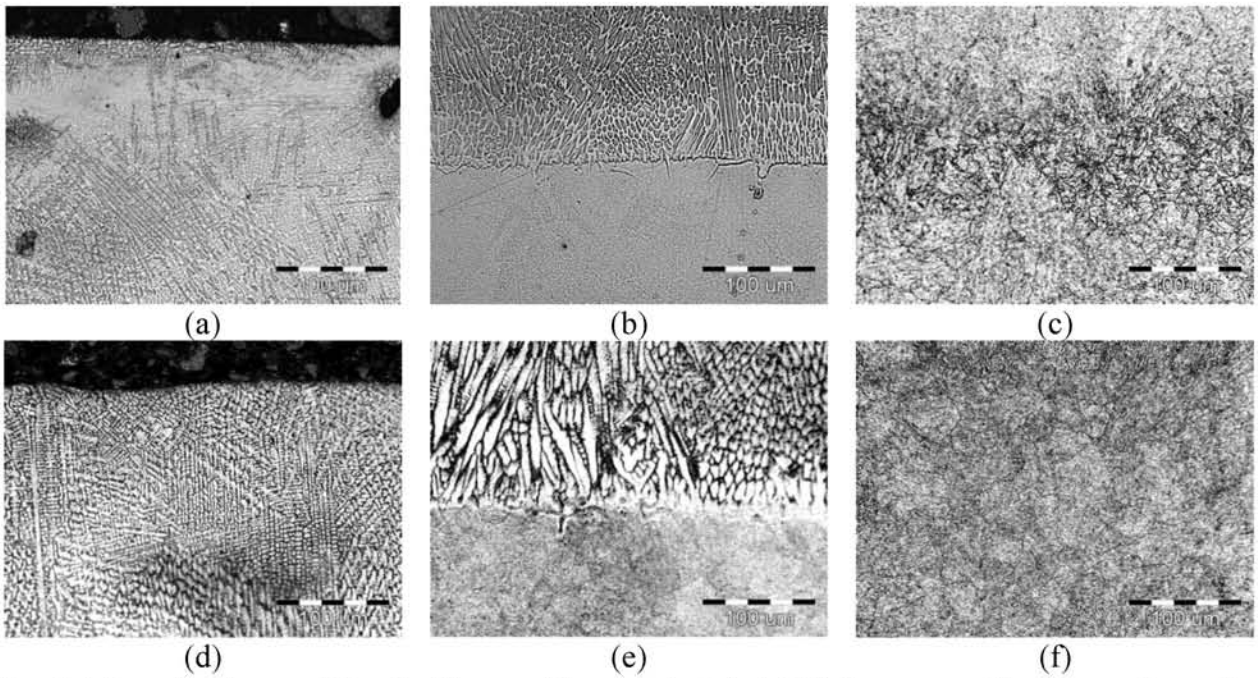

Fig. 4. Microstructures of the cladding and base material at 200-times magnification under optical microscope, etched in 10 % nital; (a) surface after cladding, (b) FZ/ HAZ boundary after cladding, (c) HAZ/heat-unaffected zone boundary, (d) surface after SA (900 °C, 1h) and PA (525 °C, 1h), (e) FZ / HAZ boundary after SA (900 °C, 1h) and PA (525 °C, 1h), (f) base material after subsequent SA (900 °C, 1h) and PA (525 °C, 1h)

Figure 4c shows the zone 1.6 mm below the clad surface, which was more intensely etched. This zone is adjacent to the heat-unaffected zone.

Figures 4(d-e-f) show the microstructure after 1h solution annealing at 900 °C (dissolution of alloying elements in austenite), and after 1h precipitation annealing (precipitation of Ni_3Ti and Ni_3Mo precipitates). Figure 4e shows a fusion boundary between the fusion zone and HAZ, which is slightly blurred after heat treatment.
The chemical analysis was made to assure the equality of chemical compositions of the clads and base material. Measuring points were located 0.1, 0.5, 1, and 2 mm below the surface. A field for a surface analysis was 140 x 120 μm in size with a magnification of 1000 times. The chemical analysis was made with JEOL JXA-8600 (SEM) electronic microscope with the addition of a microprobe for energy-dispersive spectroscopy (EDS). The microchemical analyses in the study concerned were focused on sensing the fractions of all elemental elements in the Ni-Co-Mo-Ti alloy, i.e. nickel (Ni_{28}), cobalt (Co_{27}), molybdenum (Mo_{42}), titanium (Ti_{22}), aluminium (Al_{13}), silicon (Si_{14}), and iron (Fe_{26}), except carbon (C_6) and boron (B_5), because of the sensibility limit of the microprobe. The similarity of the chemical compositions of the clad and the base material were confirmed.

3.4 Residual stresses in the surfaced layers and base material

Strain measurements and calculations of residual stresses in the surface layer were based on the relaxation hole-drilling method in accordance with ASTM standards (ASTM Int., E 837-01, 1995 and ASTM Int., E 837-08, 2008) and using measuring resistance rosettes CEA-06-062-UM and device RS-200 Milling Guide, Vishay Group. The residual-stress variation in the surfaced specimens was determined using an integral method and a program package H-drill.
Weiping [12] reports on measurements of residual stresses in parallel laser-remelted tracks where compression residual stresses occur if overlapping is narrow (10 %). Grum and Slabe [6] measured compression residual stresses with 20 % overlapping and the spiral mode of laser-beam guidance, which has a favourable influence on the resistance of components under dynamic loads. The generation of compression residual stresses is a result of phase transformation changes from an austenitic microstructure into a martensitic one due to volume differences.
Figure 5 shows variations of minimal principal residual stresses in claddings (to the depth of 0.6 mm) and in the base material to the depth of 1 mm. The values of through-depth variation of residual stress for three different modes of laser-beam guidance, i.e. in a spiral (Mode I), zig-zag (mode II) and parallel intermittent line (Mode III) with 20 % overlapping of the laser beam is shown on Fig 5. Measurements were made at two points at the clad face and clad weld, Fig. 5a and Fig 5b. All measurements confirms high compressive residual stresses which are slightly higher at the clad toe than at the clad face.

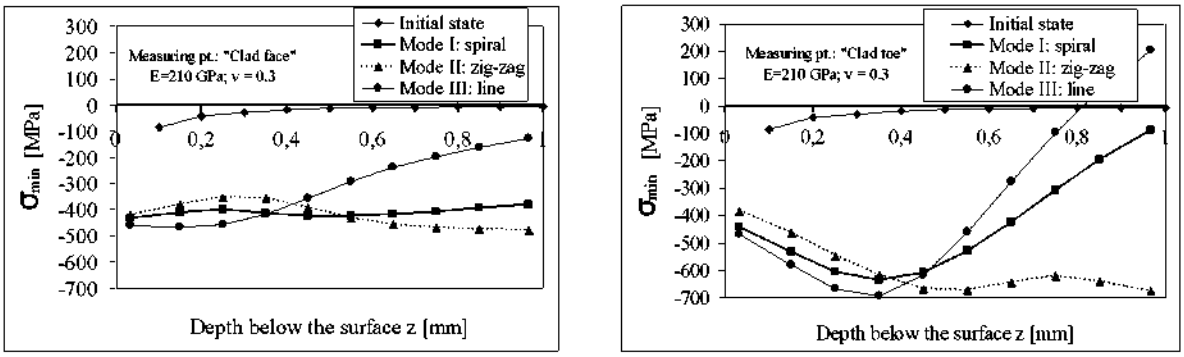

(a) clad face (b) clad toe

Fig. 5. Minimal principal residual stresses (σ_{min}) before and after laser cladding of Ni-Co-Mo powder

4. Conclusions

According to a high practicability and simplicity of the laser cladding process, efficient and cost-effective maintenance of damaged surfaces of vital parts of 1.2799 maraging steel tools for die casting can be expected. High hardness of a NiCoMo cladded layer, i.e. between 400 and 450 $HV_{0.3}$, is attained after laser cladding; therefore, there is a possibility that cladding is carried out on a precipitation-hardened material without subsequent precipitation hardening, which permits cheaper repair. Nd:YAG coaxial guidance provides good repeatability of the geometrical cross-sectional dimensions in the laser-cladding. The microstructure analysis showed a predominantly cellular dendritic microstructure at the surface and perpendicularly oriented, predominantly dendrite morphology close to the fusion line/HAZ boundary. After heat treatment the HAZ exhibits the same properties as the heat-unaffected zone. The EDS analysis shows a similar chemical composition of the surfacing weld and the base material with a slight excess of nickel in the base material and a slightly higher titanium content in the cladding. After laser cladding, high compression residual stresses were obtained in the clad face and the clad toe through the surfaced-layer depth. Such a stress state can extend operating life of a tool.

5. References

[1] B. Gehricke: Proceedings of the Conference on the Die Casting Technology in Harmony with the Environment, Cleveland, October 18-21, 1993, 209-217.

[2] R. F. Decker, S. Floreen: The Minerals, Metals&Materials Society, 1988, 1-37

[3] J.L. Ocaña, M.Morales, C. Molpeceres, J. Torres, Applied surface science 238 (2004), 242-248.

[4] J. Grum, M. Zupančič, J.L. Ocaña. Materials Science Forum Vols. 537-538 (2007), pp. 655-662

[5] V. Gliha, T. Vuherer, B. Pucko. B. Ule, J. V. Tuma; Materials and Manufacturing Processes, Vol. 19., No. 2., pp. 139-157, 2004

[6] J. Grum, J.M. Slabe: J. Mat. Proc. Tech. 155-156 (2004), pp. 2026-2032

[7] J. Grum. J.M Slabe: Surf.&Coat. Tech. 180-181 (2004), pp. 596-602

[8] C.R. Shamantha, R. Narayanan, K.J.L. Iyer, V.M. Radhakrishnan, S.K. Seshadri, S. Sundararajan, S. Sunderesan: Mat. Sci.& Eng., A287 (2000), pp. 43-51

[9] U.K. Viswanathan, G.K. Dey, V. Sethumadhavan: : Materials Science&Engineering A 398 (2005), pp. 367-372

[10] Handbook of Residual Stress and Deformation of Steel, ASM International, Editor: G. Totten, M. Howes, T. Inoue, pp. 391-396

[11] T. Vuherer, D. Rojko, V. Gliha: Materiali in tehnologije 35 (2001) pp. 1-2.

[12] C. Weiping: J. Phys.: Condens. Matter 5 (1993) L643-L646.